

# Spherical Silver Nanocrystals Arranged in a Metastable Square Pattern

Sushil Swaroop Pathak,\* Savita Priya, Gotluru Kedarnath, and Leela S. Panchakarla\*

Cite This: *ACS Omega* 2022, 7, 28481–28486

Read Online

ACCESS |



Metrics &amp; More

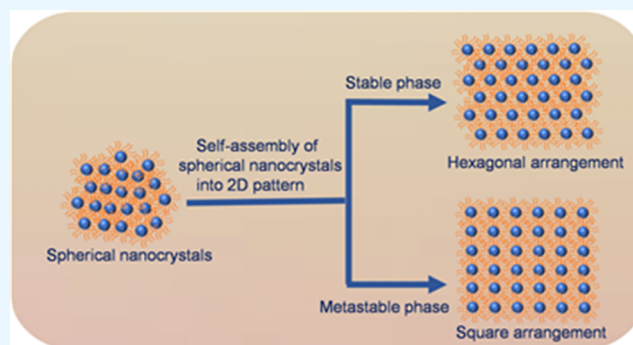


Article Recommendations



Supporting Information

**ABSTRACT:** The present article demonstrates the development of two-dimensional (2D) assembly of spherical nanocrystals (NCs) in the square arrangement through the delicate balance between repulsive ligand interactions and attractive van der Waals interactions of NCs, respectively, instead of the otherwise stable hexagonal arrangement. The experimental packing efficiency values matched quite well with the theoretically calculated square arrangement patterns. The above fact indicates that the formation of the 2D square arrangement of silver NCs can be explained by introducing the concept of softness to NCs in the hard sphere model.



## 1. INTRODUCTION

Nature forces isotropic particles to self-assemble into a more close-packed structure. Self-assembly is defined as the spontaneous organization of the distinct components due to direct specific interactions and/or indirectly via their environment. Self-assembly is a manifestation of an equilibrium between the attractive van der Waals (vdW) forces and the repulsive steric forces between colloidal nanocrystals (NCs). The formation of self-assembly depends on different forces, including vdW forces [Keesom forces (orientation force), Debye forces (induction force), and London dispersion forces], electrostatic forces, dipole–dipole interactions between the nanoparticles, entropy, and ligand–ligand interaction.<sup>1–6</sup> However, it is very challenging to assemble nanoparticles into a particular pattern because it involves not only the understanding of these intriguing interactions but also control over the shape, size of the nanoparticle building blocks and the chemical environment of the assembly.<sup>7–12</sup> A variety of nanoparticles self-assemble into ordered superlattices, among which spherical nanoparticles are widely studied both theoretically and experimentally.<sup>13–15</sup> Traditionally, the ordered structures were labeled as entropy-driven phase transitions invoking the hard sphere model.<sup>16–18</sup> The model expects close-packed face-centered cubic (fcc) or hexagonal close packing (hcp) structures for the self-assembly of these NCs with an edge to fcc structure. However, under certain conditions, both the types of hcp and fcc superlattices have been observed simultaneously, with the dominance of the hcp structure. This imparts the role of some additional forces or interactions in these ordered structures.<sup>19</sup> In fact, only some of the experimentally observed superlattice patterns assembled by colloidal NCs can be explained by the hard sphere packing

model. The latter model cannot describe several non-close-packed ordered lattices. Such a type of deviation from close-packed structures occurs because the preferred crystal structure for the superlattice not only depends on the shape of the NC (shape of the core) building blocks of the assembly but also depends on its softness arising due to the surrounding surfactant, its nature, and the range of the interaction between surrounding colloidal NCs. The incompressible inorganic core and soft corona of hydrocarbon surface ligands fit colloidal NCs between the hard and soft particle models. Therefore, many two- and three-dimensional (2D and 3D, respectively) superlattice arrangements formed by colloidal NCs with a 2–10 nm core diameter and a hydrocarbon surfactant of C<sub>8</sub>–C<sub>18</sub> chain length can be delineated by both dense packaging and contact area-minimizing configurations.<sup>20</sup> Several close-packed<sup>21</sup> and non-close-packed superlattices of metal<sup>22–24</sup> and semiconductor NCs<sup>25</sup> of different shapes and sizes have been reported, which are explained on the lines of the soft particle model introducing interactions in the discussion. For instance, Korgel et al. introduced a soft sphere model to explain close-packed 2D and 3D superlattices of dodecahedral capped silver NCs.<sup>21</sup> The same group reported non-close-packed body-centered cubic (bcc) and body-centered tetragonal structures for the alkanethiol-capped silver NC

Received: May 25, 2022

Accepted: July 25, 2022

Published: August 5, 2022



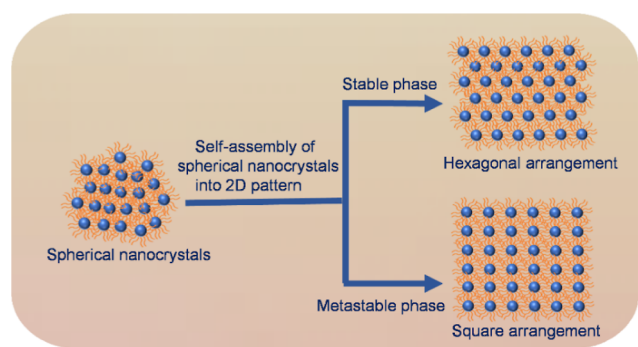
superlattice.<sup>22</sup> Demortière and co-workers elucidated the shape-dependent close-packed and non-close packed arrangement in 2D and 3D superlattices of platinum NCs.<sup>23</sup> In the present investigation, we report both hexagonal and square arrangements for 2D superlattices of oleylamine (OAm)-capped spherical silver NCs. To the best of our knowledge, the square arrangement has not been reported unambiguously for 2D superlattices of silver spherical NCs capped by OAm over a long range. However, the square arrangement of Ag NCs has been claimed in the literature.<sup>26,27</sup> Such a type of arrangement principally arises due to the effect of an equilibrium between the attractive vdW forces and the repulsive steric forces.<sup>28,29</sup>

## 2. EXPERIMENTAL SECTION

**2.1. Materials.** Octadecene (95%, Sigma-Aldrich), OAm (Loba), benzyl alcohol (99% Sigma-Aldrich), silver(I) nitrate ( $\text{AgNO}_3$ ) (99%, Sigma-Aldrich), ethanol (EtOH) (spectroscopy grade), and chloroform (high-performance liquid chromatography grade) were used.

**2.2. Synthesis of Silver NCs.** A 25 mL round-bottom flask was equipped with OAm (1.5 mL) and octadecene (1 mL), and to this mixture of solutions,  $\text{AgNO}_3$  (10 mg) in benzyl alcohol (2 mL) was added at room temperature and stirred at 60 °C under the inert condition. Further, the temperature was increased, held at 100 °C for 15 min, and then increased to 172 °C for 20 min. Therefore, the reaction mixture was cooled down to room temperature under slow cooling conditions, diluted with 15 mL of EtOH, and centrifuged twice (6000 rpm). The resulting solution was again stirred (500 rpm) at room temperature for 24 h under closed conditions. The formed solution was left undisturbed, and the particles were collected from the top layer of the sample for high-resolution transmission electron microscopy (HRTEM) analysis. The dried precipitate was separately analyzed for phase determination (Scheme 1).

### Scheme 1. Schematic Illustration of Silver Spherical NCs in a Hexagonal and Square Arrangement



**2.3. Analytical Information.** The phase purity and electronic structure analyses of the synthesized silver NCs were performed by using X-ray diffraction (XRD) analysis (Rigaku, Smartlab) and Fourier transform infrared (FTIR) spectroscopy using a Bruker Tensor 27. The UV–visible absorption spectra were recorded using a PerkinElmer Lambda 950 spectrophotometer. The assembly of silver NCs studies was characterized by HRTEM using JEM-2100F—200 kV and FEI-Tecna G2, F30—300 kV microscopes. Thermogravimetric analysis (TGA) was performed under inert ( $\text{N}_2$  flow)

conditions at the heating rate of 10 °C  $\text{min}^{-1}$  (up to 800 °C) by using a PerkinElmer Pyris 6 thermogravimetric analyzer.

## 3. RESULTS AND DISCUSSION

The Ag NCs were synthesized using  $\text{AgNO}_3$  as a silver source, to which OAm, benzyl alcohol, and octadecene were added to form a suspension, which was then heated to 60 °C and left undisturbed until the granules of  $\text{AgNO}_3$  were completely dissolved to form a colorless solution. This colorless reaction mixture demonstrates that OAm does not yet reduce the  $\text{Ag}^+$  ions. The contents of the reaction mixture were further heated to 100–120 °C for 15–20 min, followed by heating at 170–180 °C for 20–30 min. The high temperature enables OAm to reduce  $\text{Ag}^+$  drastically, indicated by the conversion of the reaction mixture to a dark solution, according to the surface plasmon resonance results of Ag NCs in the reaction mixture. Complete reduction of  $\text{Ag}^+$  ions could be attained within a few minutes, initially forming Ag NCs with a wide range of size particles. The Ostwald ripening process was employed to obtain an even distribution of particle size by increasing the duration of the reaction at higher temperature to 20–30 min. The extended incubation time of the reaction resulted in the formation of uniform spherical Ag NCs, which has been depicted in Figure 1. The centrifugation process could offer a further selection of uniform particle sizes. The synthesized Ag NC solution was centrifuged in 15 mL of EtOH at 6000 rpm twice. The Ag NCs were again stirred for 24 h at room temperature and then left to stand for a few hours to settle down. The solution in the upper layer was carefully lifted onto a Cu grid for further characterization. The TEM images revealed two different arrangements of spherical NCs, that is, hexagonal and square patterns, as shown in Figure 1a–g. The sizes of spherical NCs in hexagonal and square arrangements were  $\sim 8$  and  $\sim 4$  nm, respectively. In the hexagonal arrangement, the interparticle distance between two NCs was 2.8 nm, while in the square arrangement, the interparticle distance was different, the edge (facial) interparticle distance was 3.4 nm, and the diagonal interparticle distance was found to be 4.4 nm, as shown in Figure 1c,g. The selected area electron diffraction (SAED) indexed to the square structure with a polycrystalline nature and the HRTEM image showed the interplanar  $d$ -spacing of 0.217 nm with the facet plane (200) of Ag NPs (Figure 1h,i). Here, OAm acted as both a surfactant and a reducing agent, stabilizing the formed spherical Ag NCs. The OAm molecules produced a coating around the Ag NCs via the donation of the lone pair electron of the N atom of the amine group ( $-\text{NH}_2$ ) of OAm to the surface Ag atoms of the spherical NCs. The FTIR spectrum of the as-synthesized spherical Ag NCs, as illustrated in Figure S1 (Supporting Information), was predominantly analogous to that of pure OAm. The FTIR spectrum of Ag NCs depicted all the characteristic peaks of pure OAm with the addition of a new peak at 1540  $\text{cm}^{-1}$ , which originated from the Ag–N bond. The powder XRD pattern of Ag NCs, as illustrated in Figure S2, matches exactly with that of the pure square system (space group:  $Fm\bar{3}m$ ; JCPDS card no 04-0783). The optical properties of Ag NCs dispersed in chloroform were studied, and the observations are described in Figure S3. The absorption spectra, recorded in the range of 200–800 nm, exhibited an intense peak at 405 nm, indicating uniformity in Ag NC size. A peak in the absorption spectra of metal NCs resulted from the intra-band excitations of conduction

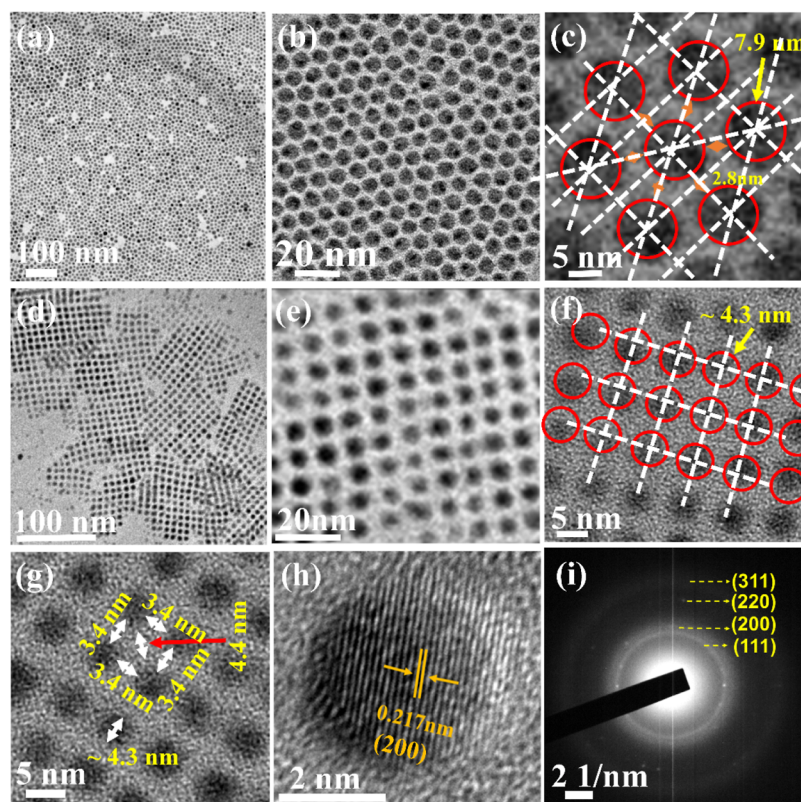


**Figure 1.** Self-assembled Ag NCs in hexagonal and square patterns synthesized using OAm. (OAm 2 mL, benzyl alcohol 4 mL, and octadecene 1 mL.) (a–c) Low- and high-magnification TEM images of the hexagonal arrangement. (d–g) Low- and high-magnification TEM images of the square arrangement. (h) HRTEM image and (i) SAED pattern of Ag NCs.

electrons from the lowest energy state to a higher energy state within the conduction band of metal NCs.<sup>30,31</sup>

The formation of both hexagonal (8 nm Ag NCs) and square arrangements (4 nm Ag NCs) of a 2D superlattice of spherical silver NCs could be elucidated with the help of NC “softness”, expressed as  $\chi = L/R$ , where  $L$  is the molecular length of the surfactant and  $R$  is the radius of the inorganic core.<sup>20</sup> This softness parameter played a significant role in choosing between close-packed and non-close-packed sphere arrangements. For instance, the Korgel group explained the stability of bcc superlattices over fcc for  $\chi > 0.7$  using the area minimization principle,<sup>32,33</sup> and the same was observed for other systems.<sup>34</sup> In the present investigation,  $\chi$  values calculated for NCs of sizes 8 and 4 nm are determined to be 0.54 and 1.08, respectively. For 8 nm Ag NCs, a simple hexagonal arrangement with a coordination number of 6 was observed in their 2D superlattice (Figures 1a–c and S4), which can be extrapolated to a close-packed arrangement in its 3D superlattice (fcc or hcp in 3D). This could further be endorsed by the softness parameter  $\chi = 0.54$ , which was less than 0.7, for which close-packed arrangements are favorable in 3D. Accordingly, for NCs of size 4 nm, which have a substantial soft character ( $\chi = 1.08$ ), contributed by surface surfactants, the arrangement of NCs was a reflection of both sphere packing and area-minimizing components. Such soft NCs could be deformed according to the coordination environment around them. The soft NCs with a lower coordination number can saturate the spaces more efficiently than the hard NCs (Figure 2) because they may adapt to a shape according to the available space, as controlled by the local coordination environment.<sup>20</sup> This has further been upheld by a lower

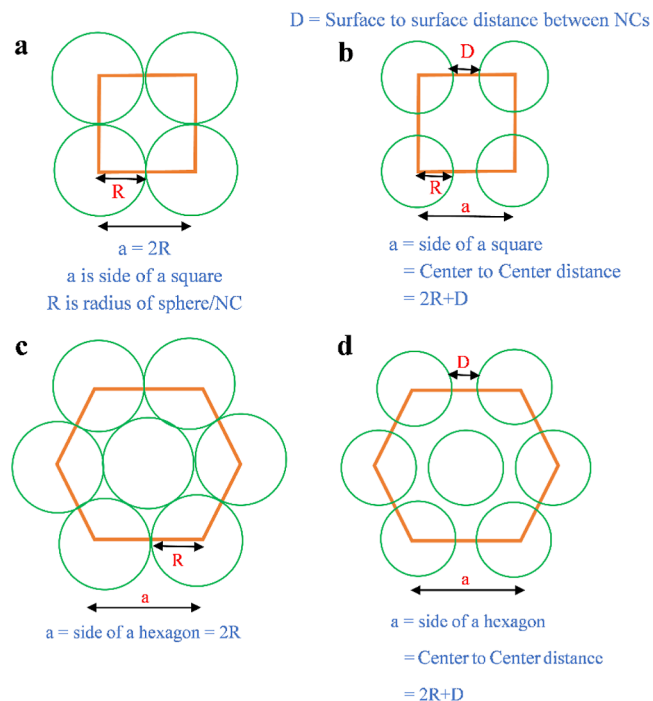


**Figure 2.** Square arrangement in (a) hard sphere model and (b) soft sphere model and hexagonal arrangement in (c) hard sphere model and (d) soft sphere model.

coordination number of 4 around the 4 nm NCs (Figures 1d–f and S5) compared to a higher coordination number of 6 around 8 nm NC (Figures 1a–c and S4). Further, it has been

observed that for  $\chi > 0.7$ , fcc or hcp were not stable and thus attempted to adopt a shape through the deformation of surfactant ligands, which densify the structure. The deformation of these soft NCs could further be confirmed by the lower interparticle distance of NCs (3.4 nm) with respect to twice the length of the surfactant ( $2L = 4.3$  nm). This indicates the presence of vdW attraction forces between the NCs.

In addition, the interparticle interactions between Ag NCs were relatively strong owing to the high polarizable nature of the Ag NC core.<sup>21</sup> The latter nature of the Ag NC core influences NCs orientation inducing an attraction force.<sup>21</sup> Such types of factors directing the NC orientation also enabled NCs to be arranged in a square pattern, which otherwise was not preferred. Moreover, the arrangement of self-assembly was mainly a consequence of an equilibrium between the attractive vdW forces and the repulsive steric forces.<sup>31</sup> For 8 nm Ag spherical NCs, these forces were isotropic, resulting in a 2D hexagonal pattern, while the anisotropic forces, as in the case of 4 nm Ag NCs, ensure a 2D square arrangement. Having the information on the OAm coverage on the NC surface, the steric repulsion energy ( $E_{\text{steric}}$ ) and long-range vdW attraction between two OAm-capped Ag NCs could be calculated using de Gennes and Hamaker expressions, respectively, for two dense layers of strongly adsorbed chains in a good solvent.<sup>21</sup>

de Gennes expression

$$E_{\text{steric}} = \frac{100R\delta^2}{(C - 2R)\pi\sigma_{\text{amine}}^3} kT \exp\left(\frac{-\pi(C - 2R)}{\delta}\right)$$

where  $\delta$  is the brush thickness (21.47 Å),<sup>20</sup>  $R$  is the radius of the NC (20 Å), and  $\sigma_{\text{amine}}$  is the diameter of the area occupied by OAm on the particle surface (6.8 Å).<sup>20</sup>

Hamaker expression

$$E_{\text{vdw}} = \frac{-A}{12} \left\{ \frac{4R^2}{C^2 - 4R^2} + \frac{4R^2}{C^2} + \ln\left[\frac{C^2 - 4R^2}{C^2}\right] \right\}$$

where  $A$  is the Hamaker constant (1.95 eV)<sup>21</sup> and  $C$  is the center-to-center distance between NCs (34 Å). The interaction potential, which included both steric repulsion and the long-range vdW attraction between two OAm-capped Ag NCs, could be calculated by the summation of de Gennes and Hamaker expressions.

It is known that an attractive interactive potential/potential well has been formed as a consequence of the competition between long-ranged vdW attraction and short-ranged steric repulsion.<sup>35</sup> The location and depth of the attraction potential well were controlled by the particle size, Hamaker constant, and ligand coverage.<sup>35</sup> For small particle sizes, such as that in the present investigation (40 Å), the potential well was too small, and a very weak interaction potential ( $-4.2 \times 10^{-5}$  eV) has been observed at a center-to-center distance of 84 Å. Beyond this point, steric repulsion ( $E_{\text{steric}}$ ) dominates over vdW attraction and prevents particles from forming kinetically trapped aggregates. At this optimum center-to-center distance of 84 Å, the Ag NCs are arranged in a square assembly, which was in close agreement with the center-to-center distance of 74 Å, as calculated from the TEM image (Figure 1g). A sharp increase in  $E_{\text{steric}}$  governs the interaction potential at separations less than 44 Å (Figure 3), indicating that Ag NCs experienced a strong steric repulsion with the neighboring NCs even before the surface of NCs touched each other (at this point, the center to center distance is  $\sim 40$  Å). This

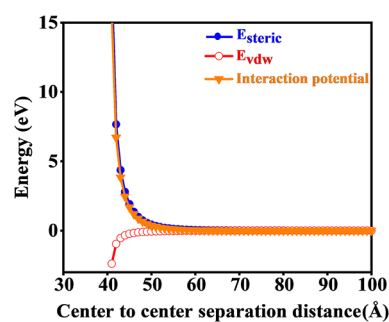


**Figure 3.** Interparticle potential ( $V$ ) between two OAm-capped 40 Å diameter Ag NCs:  $E_{\text{steric}}$  ( $\bullet$ ) plotted using the de Gennes expression and  $E_{\text{vdw}}$  ( $\circ$ ) plotted using the Hamaker expression.

suggested that 40 Å Ag NCs have an effective particle size of 44 Å or an effective radius of 22 Å, which extended 2 Å beyond the core radius of Ag NCs (20 Å). This type of effective radius was observed for thiol-capped Ag NCs.<sup>36</sup>

Along with the above factors, the possible scenario for the appearance of two types of 2D arrangement could be rationalized by the evaporation effect of the deposition of two different sizes (4 and 8 nm) of Ag NCs having different graft densities, which thereafter facilitated the varying interparticle interactions along with the interactions of the NCs and surface ligands with the carbon surface of the TEM grid. In the present report, Ag NCs redispersed in EtOH were lifted onto an amorphous carbon-coated copper TEM grid and slowly evaporated for 24 h. The slow evaporation of EtOH dispersion of Ag NCs containing two different particle size populations with varying graft densities (graft densities of 4 and 8 nm size Ag NCs are 14.98 and 2.09 ligands/nm<sup>2</sup>, respectively) allowed the inorganic cores and ligands of NCs to interact differently with the surface of the substrate and the neighboring NCs in such a way that 4 and 8 nm Ag NCs are arranged in 2D square and hexagonal patterns, respectively. This type of variable interaction was the consequence of the significant participation of the substrate surface in the deformation shell and particle interactions.

The theoretical and experimental packing efficiency (PE) for 2D square and 2D hexagonal arrangements of Ag NCs has also been calculated assuming full coverage (100% coverage) of the ligand/surfactant on the Ag NC surface (for calculations, see the Supporting Information). Theoretical and experimental PE values for square and hexagonal arrangements were 78 and 72.1% (PE of NC + PE of the surfactant = 22.9 + 49.2% = 72.1%) and 91 and 103% (PE of NC + PE of the surfactant = 49.7% + 53.3% = 103%), respectively. Theoretical and experimental PE values for the square arrangement were in close agreement with each other, indicating that the formation of square arrangements of 2D superlattices of Ag NCs could be explained by invoking the softness of NCs in the hard sphere model (Figure 3). On other hand, an experimental PE greater than 100% pointed out the fact that the better explanation of hexagonal arrangement is the hard sphere model.

Further, to find out the precise experimental PE for the 2D square arrangement of Ag NCs, the exact fractional coverage of the surfactant or ligand (organic fraction) on the surface of Ag NCs was determined by TGA of the Ag NCs of size 4 nm (Figure S6). The TGA showed a three-step decomposition corresponding to loosely and strongly bound organic ligands passivating the surface of Ag NCs. The measured organic fraction (weight loss of 19.2%) was used to calculate the

precise experimental PE for the 2D square arrangement of Ag NCs (for calculations, see the Supporting Information), which were determined to be 68%. This experimental value (68%) was comparable to the theoretical PE for the 2D square arrangement (78%), which endorsed the 2D square arrangement of Ag NCs.

Last but not the least, the kinetic factors<sup>19</sup> could also lead to the metastable product with the 2D square arrangement along with the major product with a 2D hexagonal arrangement. The relative areas of the hexagonal and square arrangements are depicted in different frames/TEM images, as shown in Figure S7 and Table S1.

The experimental space-filling fraction or PE of the 2D square arrangement is calculated by using the organic mass fraction obtained from TGA

$$\begin{aligned} \text{volume of NC } (V_{\text{NC}}) &= (4/3)\pi R^3 \\ &= (4/3) \times 3.14 \times (2 \times 10^{-7})^3 \\ &= 33.49 \times 10^{-21} \text{ cm}^3/\text{NC} \\ (\text{Taking } R &= 20 \text{ \AA} \text{ or } 2 \times 10^{-7} \text{ cm}) \\ m_{\text{NC}} &= V_{\text{NC}} \times \rho_{\text{Ag}} = 33.49 \times 10^{-21} \text{ cm}^3/\text{NC} \times 10.49 \\ &\text{ g/cm}^3 = 3.51 \times 10^{-19} \text{ g/NC} \end{aligned}$$

$$\begin{aligned} m_{\text{NC+ligand}} &= \\ &= \frac{m_{\text{NC}}}{1 - \text{organic mass fraction obtained from TGA}} \\ &= \frac{3.51 \times 10^{-19} \text{ g/NC}}{1 - 0.192} \\ &= 4.34 \times 10^{-19} \text{ g/NC} \end{aligned}$$

$$\begin{aligned} m_{\text{ligand}} &= m_{\text{NC+ligand}} - m_{\text{NC}} = 0.83 \times 10^{-19} \text{ g/NC} \\ \text{volume of the ligand shell } (V_{\text{ligand}}) &= m_{\text{ligand}} / \rho_{\text{ligand}} \\ &= 0.83 \times 10^{-19} \text{ g/NC} / 0.84 \text{ g/cm}^3 \\ &= 0.988 \times 10^{-19} \text{ cm}^3 = 98.8 \text{ nm}^3 \end{aligned}$$

(Taking density of frozen OAm = 0.84 g/cm<sup>3</sup>).

Percentage coverage of the NC surface by the ligand = volume of the ligand shell / (N<sub>ligand</sub> × theoretical volume of the ligand)

$$\begin{aligned} \text{percentage coverage of the NC surface by the ligand} &= \\ &= \frac{\text{volume of the ligand shell}}{N_{\text{ligand}} \times \text{theoretical volume of the ligand}} \times 100 \\ &= \frac{98.8}{\frac{4\pi R^2}{\pi r_{\text{ligand}}^2} \times \pi r_{\text{ligand}}^2 h} \times 100 \\ &= \frac{98.8}{4\pi R^2 h} \times 100 \\ &= \frac{98.8}{4\pi \times 2^2 \times h} \times 100 \end{aligned}$$

$$\begin{aligned} &= \frac{98.8}{107.76} \times 100 \\ &= 91.68\% \end{aligned}$$

(Considering the shape of the ligand as cylindrical, theoretical volume of the ligand was given by  $\pi r_{\text{ligand}}^2 h$ , where  $r_{\text{ligand}}$  is the radius of the ligand head and  $h$  is the ligand height.)

Now, taking the fractional coverage of the NC surface by the ligand = 0.917,

Experimental PE of the ligand = (fractional coverage of the NC surface by the ligand × PE of the ligand obtained by observed values) = 0.917 × 49.2% = 45.1%.

Experimental PE of the 2D square arrangement = PE of the NC + PE of the ligand = 22.9 + 45.1 = 68%.

Theoretical PE of the 2D square arrangement = 78%

## 4. CONCLUSIONS

The 2D square superlattice arrangement via self-assembly of silver NCs has been rationalized over the more favorable 2D hexagonal superlattices. The softness of 4 nm Ag NCs has been affirmed by calculating the interaction potential using de Gennes and Hamaker expressions. Furthermore, the calculated theoretical and observed experimental PE values for square arrangements provided similar outcomes. Hence, it is indicated that the formation of the 2D square arrangement of superlattices of Ag NCs could be validated by introducing the concept of softness to NCs in the hard sphere model.

## ■ ASSOCIATED CONTENT

### Supporting Information

The Supporting Information is available free of charge at <https://pubs.acs.org/doi/10.1021/acsomega.2c03259>.

Infrared spectra, XRD patterns, UV spectra, TEM images, TGA curves, and calculations (PDF)

## ■ AUTHOR INFORMATION

### Corresponding Authors

**Sushil Swaroop Pathak** – Department of Chemistry, Indian Institute of Technology Bombay, Powai, Mumbai 400076, India; [orcid.org/0000-0001-5166-7970](https://orcid.org/0000-0001-5166-7970); Email: [164033049@iitb.ac.in](mailto:164033049@iitb.ac.in)

**Leela S. Panchakarla** – Department of Chemistry, Indian Institute of Technology Bombay, Powai, Mumbai 400076, India; [orcid.org/0000-0001-5829-3377](https://orcid.org/0000-0001-5829-3377); Email: [panchakarla@chem.iitb.ac.in](mailto:panchakarla@chem.iitb.ac.in)

### Authors

**Savita Priya** – Department of Chemistry, Indian Institute of Technology Bombay, Powai, Mumbai 400076, India

**Gotluru Kedarnath** – Chemistry Division, Bhabha Atomic Research Centre, Mumbai 400085, India; Homi Bhabha National Institute, Mumbai 400094, India

Complete contact information is available at:

<https://pubs.acs.org/doi/10.1021/acsomega.2c03259>

### Notes

The authors declare no competing financial interest.

## ■ ACKNOWLEDGMENTS

The authors acknowledge the Department of Chemistry, Indian Institute of Technology (IIT) Bombay and the Science

and Engineering Research Board under the Department of Science and Technology (DST-SERB), Government of India for funding (EMR/2016/003594). The authors thank the Sophisticated Analytical Instrument Facility (SAIF), IIT Bombay, Industrial Research and Consultancy Center (IRCC), IIT Bombay for all the facilities provided. SSP and SP thank CSIR and PMRF for the fellowship.

## REFERENCES

- (1) Batista, C. A. S.; Larson, R. G.; Kotov, N. A. Nonadditivity of Nanoparticle Interactions. *Science* **2015**, *350*, 1242477.
- (2) Min, Y.; Akbulut, M.; Kristiansen, K.; Golan, Y.; Israelachvili, J. The Role of Interparticle and External Forces in Nanoparticle Assembly. *Nat. Mater.* **2008**, *7*, 527–538.
- (3) Bishop, K. J. M.; Wilmer, C. E.; Soh, S.; Grzybowski, B. A. Nanoscale Forces and Their Uses in Self-assembly. *Small* **2009**, *5*, 1600–1630.
- (4) Hwang, B. H.; Ahn, H. J.; Rho, S. J.; Chae, S. S.; Baik, H. K. Vertical Alignment of Liquid Crystals with Negative Dielectric Anisotropy on an Inorganic Thin Film with a Hydrophilic Surface. *Langmuir* **2009**, *25*, 8306–8312.
- (5) Castelli, A.; de Graaf, J.; Marras, S.; Brescia, R.; Goldoni, L.; Manna, L.; Arciniegas, M. P. Understanding and Tailoring Ligand Interactions in the Self-Assembly of Branched Colloidal Nanocrystals into Planar Superlattices. *Nat. Commun.* **2018**, *9*, 1141.
- (6) Boles, M. A.; Engel, M.; Talapin, D. V. Self-Assembly of Colloidal Nanocrystals: From Intricate Structures to Functional Materials. *Chem. Rev.* **2016**, *116*, 11220–11289.
- (7) Adhikari, B.; Kraatz, H.-B. Redox-Triggered Changes in the Self-Assembly of a Ferrocene–Peptide Conjugate. *Chem. Commun.* **2014**, *50*, 5551–5553.
- (8) Shevchenko, E. V.; Talapin, D. V.; Kotov, N. A.; O'Brien, S.; Murray, C. B. Structural Diversity in Binary Nanoparticle Superlattices. *Nature* **2006**, *439*, 55–59.
- (9) Redl, F. X.; Cho, K.-S.; Murray, C. B.; O'Brien, S. Three-Dimensional Binary Superlattices of Magnetic Nanocrystals and Semiconductor Quantum Dots. *Nature* **2003**, *423*, 968–971.
- (10) Agarwal, U.; Escobedo, F. A. Mesophase Behaviour of Polyhedral Particles. *Nat. Mater.* **2011**, *10*, 230–235.
- (11) Pileni, M. P. Control of the Size and Shape of Inorganic Nanocrystals at Various Scales from Nano to Macrod domains. *J. Phys. Chem. C* **2007**, *111*, 9019–9038.
- (12) Song, Q.; Ding, Y.; Wang, Z. L.; Zhang, Z. J. Formation of Orientation-Ordered Superlattices of Magnetite Magnetic Nanocrystals from Shape-Segregated Self-Assemblies. *J. Phys. Chem. B* **2006**, *110*, 25547–25550.
- (13) Alder, B. J.; Hoover, W. G.; Young, D. A. Studies in Molecular Dynamics. V. High-density Equation of State and Entropy for Hard Disks and Spheres. *J. Chem. Phys.* **1968**, *49*, 3688–3696.
- (14) Bolhuis, P. G.; Frenkel, D.; Mau, S.-C.; Huse, D. A. Entropy Difference between Crystal Phases. *Nature* **1997**, *388*, 235–236.
- (15) Rudd, R. E.; Broughton, J. Q. Coarse-Grained Molecular Dynamics and the Atomic Limit of Finite Elements. *Phys. Rev. B: Condens. Matter Mater. Phys.* **1998**, *58*, R5893.
- (16) Gast, A. P.; Russel, W. B. Colloidal Particles Suspended in Solution Provide Intriguing Models for Studying Phase Transitions. *Phys. Today* **1998**, *51*, 24–30.
- (17) Robbins, M. O.; Kremer, K.; Grest, G. S. Phase Diagram and Dynamics of Yukawa Systems. *J. Chem. Phys.* **1988**, *88*, 3286–3312.
- (18) Russel, W. B.; Chaikin, P. M.; Zhu, J.; Meyer, W. V.; Rogers, R. Dendritic Growth of Hard Sphere Crystals. *Langmuir* **1997**, *13*, 3871–3881.
- (19) Talapin, D. V.; Shevchenko, E. V.; Murray, C. B.; Titov, A. V.; Král, P. Dipole–Dipole Interactions in Nanoparticle Superlattices. *Nano Lett.* **2007**, *7*, 1213–1219.
- (20) Borges, J.; Ribeiro, J. A.; Pereira, E. M.; Carreira, C. A.; Pereira, C. M.; Silva, F. Preparation and Characterization of DNA Films Using Oleylamine Modified Au Surfaces. *J. Colloid Interface Sci.* **2011**, *358*, 626–634.
- (21) Korgel, B. A.; Fullam, S.; Connolly, S.; Fitzmaurice, D. Assembly and Self-Organization of Silver Nanocrystal Superlattices: Ordered “Soft Spheres.”. *J. Phys. Chem. B* **1998**, *102*, 8379–8388.
- (22) Korgel, B. A.; Fitzmaurice, D. Small-Angle x-Ray-Scattering Study of Silver-Nanocrystal Disorder-Order Phase Transitions. *Phys. Rev. B: Condens. Matter Mater. Phys.* **1999**, *59*, 14191.
- (23) Demortière, A.; Launois, P.; Goubet, N.; Albouy, P.-A.; Petit, C. Shape-Controlled Platinum Nanocubes and Their Assembly into Two-Dimensional and Three-Dimensional Superlattices. *J. Phys. Chem. B* **2008**, *112*, 14583–14592.
- (24) Courty, A.; Richardi, J.; Albouy, P.-A.; Pileni, M.-P. How to Control the Crystalline Structure of Supracrystals of 5-Nm Silver Nanocrystals. *Chem. Mater.* **2011**, *23*, 4186–4192.
- (25) Murray, C. B.; Kagan, C. R.; Bawendi, M. G. Self-Organization of CdSe Nanocrystallites into Three-Dimensional Quantum Dot Superlattices. *Science* **1995**, *270*, 1335–1338.
- (26) Wang, L. Z.; Shi, J. L.; Zhang, W. H.; Ruan, M. L.; Yu, J.; Yan, D.-S. Self-Organization of Ordered Silver Nanocrystal Arrays on Cubic Mesoporous Silica Surfaces. *Chem. Mater.* **1999**, *11*, 3015–3017.
- (27) Taleb, A.; Petit, C.; Pileni, M. P. Synthesis of Highly Monodisperse Silver Nanoparticles from AOT Reverse Micelles: A Way to 2D and 3D Self-Organization. *Chem. Mater.* **1997**, *9*, 950–959.
- (28) Motte, L.; Billoudet, F.; Pileni, M. P. Self-Assembled Monolayer of Nanosized Particles Differing by Their Sizes. *J. Phys. Chem.* **1995**, *99*, 16425–16429.
- (29) Motte, L.; Billoudet, F.; Lacaze, E.; Douin, J.; Pileni, M. P. Self-Organization into 2D and 3D Superlattices of Nanosized Particles Differing by Their Size. *J. Phys. Chem. B* **1997**, *101*, 138–144.
- (30) Gharibshahi, E.; Saion, E. Quantum Mechanical Calculation of Optical Absorption of Silver and Gold Nanoparticles by Density Functional Theory. *Phys. Int.* **2010**, *1*, 57–64.
- (31) Ho, N. T.; Tien, H. N.; Jang, S.-J.; Senthilkumar, V.; Park, Y. C.; Cho, S.; Kim, Y. S. Enhancement of Recombination Process Using Silver and Graphene Quantum Dot Embedded Intermediate Layer for Efficient Organic Tandem Cells. *Sci. Rep.* **2016**, *6*, 30327.
- (32) Goodfellow, B. W.; Yu, Y.; Bosoy, C. A.; Smilgies, D.-M.; Korgel, B. A. The Role of Ligand Packing Frustration in Body-Centered Cubic (Bcc) Superlattices of Colloidal Nanocrystals. *J. Phys. Chem. Lett.* **2015**, *6*, 2406–2412.
- (33) Zihler, P.; Kamien, R. D. Maximizing Entropy by Minimizing Area: Towards a New Principle of Self-Organization. *J. Phys. Chem. B* **2001**, *105*, 10147–10158.
- (34) Thaner, R. V.; Kim, Y.; Li, T. I. N. G.; Macfarlane, R. J.; Nguyen, S. T.; de la Cruz, M. O.; Mirkin, C. A. Entropy-Driven Crystallization Behavior in DNA-Mediated Nanoparticle Assembly. *Nano Lett.* **2015**, *15*, 5545–5551.
- (35) Wu, L.; Willis, J. J.; McKay, I. S.; Diroll, B. T.; Qin, J.; Cargnello, M.; Tassone, C. J. High-Temperature Crystallization of Nanocrystals into Three-Dimensional Superlattices. *Nature* **2017**, *548*, 197–201.
- (36) Whetten, R. L.; Shafiqullin, M. N.; Khoury, J. T.; Schaaff, T. G.; Vezmar, I.; Alvarez, M. M.; Wilkinson, A. Crystal Structures of Molecular Gold Nanocrystal Arrays. *Acc. Chem. Res.* **1999**, *32*, 397–406.